Dynamic Contact Angles and Hysteresis under Electrowetting-on-Dielectric

3 AUTHORS, INCLUDING:

Wyatt Nelson
Fred Hutchinson Cancer Research Center

20 PUBLICATIONS **281** CITATIONS

SEE PROFILE

Chang-Jin Kim
University of California, Los Angeles

256 PUBLICATIONS **7,928** CITATIONS

SEE PROFILE

Dynamic Contact Angles and Hysteresis under Electrowetting-on-Dielectric

Wyatt C. Nelson[*], **Prosenjit Sen**, and **Chang-Jin "CJ" Kim**
Mechanical and Aerospace Engineering Department University of California, Los Angeles (UCLA)

Abstract

By designing and implementing a new experimental method, we have measured the dynamic advancing and receding contact angles and the resulting hysteresis of droplets under electrowetting-on-dielectric (EWOD). Measurements were obtained over wide ranges of applied EWOD voltages, or electrowetting numbers ($0 \le Ew \le 0.9$), and droplet sliding speeds, or capillary numbers ($1.4 \times 10^{-5} \le Ca \le 6.9 \times 10^{-3}$). If Ew or Ca is low, dynamic contact angle hysteresis is not affected much by the EWOD voltage or the sliding speed, i.e., the hysteresis increases by less than 50% with a two order-of-magnitude increase in sliding speed when $Ca < 10^{-3}$. If both Ew and Ca are high, however, the hysteresis increases with either the EWOD voltage or the sliding speed. Stick-slip oscillations were observed at $Ew > 0.4$. Data are interpreted with simplified hydrodynamic (Cox-Voinov) and molecular-kinetic theory (MKT) models; the Cox-Voinov model captures the trend of the data, but yields unreasonable fitting parameters. MKT fitting parameters associated with the advancing contact line are reasonable, but a lack of symmetry indicates that a more intricate model is required.

Introduction

When the characteristic dimension of a droplet is lower than the capillary length $\lambda_c = (\gamma/\rho g)^{1/2}$, (e.g., ~2.7 mm for water in air, where γ is liquid-fluid[1] surface tension, ρ the liquid density, and g the acceleration due to gravity) the static resistance to sliding along a solid surface can be quantified by contact angle hysteresis. If, for example, a capillary tube containing a droplet, or plug, of liquid is all of the sudden turned vertically, causing the liquid slowly slide downward under gravity, then the contact angles at the top and bottom of the liquid at the very moment the contact lines begin to move represent, respectively, the static receding and advancing contact angles $\theta_{r,s}$ and $\theta_{a,s}$ (the subscript 's' indicates that these are static angles), i.e., the maximum and minimum angles reached just before the contact line recedes or advances. In this case, the following expression describes the hysteresis force per unit length along the inner circumference of the tube: $f_{\text{hyst}} = \gamma (\cos\theta_{r,s} - \cos\theta_{a,s})$. In other words, contact angle hysteresis is observed because a threshold force is required to start a droplet sliding. Once sliding, the droplet exhibits dynamic advancing and receding contact angles θ_a and θ_r, and force must be continually applied to maintain the sliding against the dynamic hysteresis. To clarify further, contact angle hysteresis specifies a threshold resistance force to initial movement, and dynamic contact angle hysteresis refers to the resistance at a particular sliding speed. We found selected works of de Gennes[1, 2],

---

[*]wyattnelson@ucla.edu

[1]The liquid-fluid interface can be liquid-gas, liquid-vapor, or liquid-liquid if immiscible liquids. However, all the experiments in this report have been done with a liquid-gas system of water in air.

Supporting Information: The supporting information for this article contains: (S.1) time histories of contact angles for six medium sliding speeds, (S.2) a simple scaling analysis of low- and high-Ca oscillations, and (S.3) an analysis of simplified Cox-Voinov and MKT dynamic contact angle models. This information is available free of charge via the Internet at http://pubs.acs.org.

Robbins and Joanny[3], and Gao and McCarthy[4] to be excellent resources on the physics of contact angle hysteresis. Here we use the term 'sliding' to simply refer to the macroscopically observed motion of a droplet moving along a surface; we do not mean to imply anything about the underlying physical mechanism, e.g., we are not implying that there is slippage at the liquid-solid interface. It has been shown that dc EWOD voltages under a certain limit do not significantly affect hysteresis measured by a droplet filling and depleting experiment. Specifically, the difference between advancing and receding contact angles was approximately equal for various *Ew* up to 0.12.[5] Our investigation expands on this result by providing a full data set showing how hysteresis varies with voltage and speed in an operating condition relevant to a range EWOD-based systems, e.g., digital microfluidics,[6-8] active windows,[9] and optical displays.[10]

When quantifying the total resistance by hysteresis on a sliding droplet, one must consider the following. Typical experiments measure the dynamic contact angles θ at only two locations, e.g. θ_a at the front- and θ_r at the rear-most points of the sliding droplet, and therefore assumptions must be made to account for the variations of contact angle along the rest of the contact line. Also, the shape of the contact line must be either assumed or independently measured. A further complication is the fact that θ_a and θ_r and contact line shape are dependent on the sliding speed, or capillary number $Ca = \eta v/\gamma$, where η is shear viscosity and v is sliding velocity.[11-13] With respect to our experiments, θ_a and θ_r are used to specify the dynamic contact angle hysteresis at a single plane only: the cross-section oriented parallel to the sliding direction and passing through the center of the droplet. From the assumption that these measured angles represent extremes, we can draw useful conclusions about the total resistance on the droplet without needing to quantify the total force.

One of our main interests is to understand whether or not the pinning and de-pinning mechanisms (i.e., the causes of contact angle hysteresis) are affected by the electric fields applied during EWOD actuation. Previous studies[5, 9] suggest that, under typical EWOD conditions of an aqueous droplet on a hydrophobic surface, contact line drag is not sensitive to the applied voltage. This result implies that the drag experienced by an EWOD-actuated droplet is not sensitive to voltage, or electrowetting number $Ew = cV^2/2\gamma$, where c is specific capacitance and V is applied voltage. In other words, because the interfacial properties that cause hysteresis do not appear to change with voltage, the drag on the droplet should be expected to vary with speed only. Of course, if EWOD actuates the droplet, droplet speed and apparent contact angle are functions of *Ew*, making it difficult to isolate the EWOD effect and the speed effect – this is why we have designed experiments that do not rely on EWOD actuation for sliding and thereby enable the examination of a wide range of well controlled voltages and sliding speeds.

Schertzer et al.[14] recently reported on the dynamics of droplet transport by EWOD actuation in typical parallel-plate digital microfluidic devices. Their measurements of dynamic contact angles covered the entire process of droplet actuation, capturing acceleration, steady droplet motion, and deceleration. To provide a visual contrast, Figures 1a and 1c show schematics of EWOD actuation and our experimental setup. Despite the resemblance (i.e., the parallel-plate configuration), it is important to note a few differences that impact how our data should be interpreted. For example, we measured the contact angles of a droplet that was sliding by independent mechanical forcing, so that the entire contact line of the droplet was under the same EWOD voltage. In this way, the dynamic hysteresis we report indicates the drag forces on the droplet under EWOD without being distorted by the EWOD driving force. The EWOD pulling forces act equally in all directions (e.g., forward and backward) and therefore cancel out of the force balance. In comparison, Schertzer et al. report a hysteresis that is strongly dependent on voltage because advancing contact line is under

EWOD voltage and the receding contact line is not. Importantly, Schertzer et al. used ac voltage for actuation, which may lead to different hysteresis as that exhibited by droplets under dc EWOD.[5] Finally, droplets under EWOD actuation travel at a range of speeds – we have intentionally avoided this in our experiments in order to achieve measurements at controlled sliding speeds. This will be discussed in more detail later.

Again referring to Figure 1, let us point out another key difference between the two scenarios: the top plate in Figure 1a is hydrophobic, and the top plate in Figure 1c is hydrophilic. The main consequence of this is that the meniscus curvatures, being functions of the top and bottom contact angles as well as the distance between the plates (1 mm), will be significantly different for each case. To eliminate the effects of this coupling between the top and bottom contact angles via the meniscus curvature, we measured the contact angles less than ~50 μm from the contact line.

The scheme of forced wetting in the presence of EWOD reported here is similar to that of Blake et al.,[15] except that we covered a lower range of Ca and measured both advancing and receding angles in order to make the results more readily applicable to droplet sliding applications; Blake et al. covered a relatively high Ca range and measured only advancing angles, ensuring that the results were relevant to coating applications. Unlike coating films, EWOD-actuated droplets, e.g., in a digital microfluidic device, travel at a range of speeds during each actuation, i.e., upon the application of EWOD voltage, they accelerate to a maximum speed (reported speeds of up to ~200 mm/s) and may or may not sustain a steady speed before deceleration.[14] In our experiments, however, the transient spreading dynamics that occur upon the application of EWOD voltage are intentionally avoided. To do this, we observed droplets sliding on a steadily moving surface by employing the following procedure: (i) apply dc voltage, (ii) initiate the programmed stage movement and trigger the camera, and (ii) analyze only those video frames captured after the stage has reached a steady speed. We thus minimized inertial effects (even though they were observed in some cases at high speeds and voltages), and measured contact angles using meniscus profiles that were approximately quasi-static over the measurement duration (125 ms). Inertial effects are discussed in more detail below.

Contact angle hysteresis poses a threshold resistance to droplet motion, and it therefore determines the minimum operating voltage of EWOD chips. For example, transporting water droplets surrounded by air using a typical EWOD device (e.g. having a 1 μm thick dielectric) requires at least 20 to 30 volts. Low-voltage EWOD has been demonstrated in research settings using special high-k dielectrics and multi-layer materials.[16-19] Parallel to developing better dielectrics, gaining a better understanding of hysteresis under EWOD through experiments will provide new insights applicable to a wide range of digital microfluidic schemes,[20] e.g., using electrical,[6-8, 21-24] thermal,[25-28] or chemical[29] means to drive droplets. For example, Li and Mugele[5] demonstrated a significant reduction in contact angle hysteresis of droplets in air upon switching the actuation voltage from direct to alternating current. Oil is often used to reduce contact angle hysteresis and thus to make EWOD actuation both achievable at lower voltages and less sensitive to surface roughness. Ren et al. analyzed translation of droplets immersed in oil,[30] and Baviere et al. tracked droplets sliding by EWOD on an oil film.[21] We used dc voltages and excluded oil in our tests to avoid further complicating the dynamics resulting from time-varying forces and drag at the fluid-fluid interface.

The lack of complete theoretical understanding of wetting dynamics under basic conditions makes it difficult to build a model that accounts for all aspects of contact line motion, including capillary oscillations and the electric fields present during EWOD. There exists a range of models incorporating molecular phenomenon of the moving wetting line,[15, 31, 32]

viscous losses in the liquid body,[2, 33] and combinations of both.[34] The fact that hybrid models are often more robust is an indication that there are multiple flow regimes in which different mechanisms dominate, depending on Ca, surface energies, etc, and this is consistent with tilted plate droplet sliding[11, 35, 36] and inflation/deflation[37] experiments. The current experimental study, which builds upon preliminary work,[38] provides empirical knowledge of how resistance forces are related to electrowetting voltage and droplet sliding speed. The reported data has relevance, for example, to numerical modeling of EWOD droplet actuation. Walker et al.[39, 40] have demonstrated that accurate simulations cannot be achieved without incorporating hysteresis into such models. While our goal in this report is not to validate or modify existing theoretical models, the reported data may be useful in doing so. We have performed curve fitting using standard hydrodynamic (Cox-Voinov) and molecular-kinetic theory (MKT) models (details in Supporting Information) in order to facilitate comparisons of our data with other reports.

Experiments

The experiment was designed to measure dynamic contact angles of droplets sliding at steady speeds. Figure 1 provides simplified top and cross section views of the droplet during experiments. Here, EWOD forces are applied equally around the lower contact line of the droplet, and sliding is driven by independent mechanical means. Two important consequences of this method are as follows. First, our setup avoids the problem of tracking a moving droplet by instead observing a stationary droplet sitting on a moving surface. Second, well controlled speeds are achieved by the computer controlled actuator on which the lower substrate is mounted. In contrast, using EWOD actuation to achieve the tested range of speeds would have been very difficult, especially since we were trying to avoid transient effects.

In most cases, the top contact angles (θ_{t1} and θ_{t2}) were not dynamic contact angles because contact lines are not sliding on the top plate, which is stationary. At high voltage (60 V_{DC}, $Ew = 0.9$) and high speeds ($v > 100$ mm/s, $Ca > 1.4 \times 10^{-3}$), however, bulk oscillations of the droplet were accompanied by relocations of the top contact lines. Our main interest, i.e., dynamic contact angles under EWOD, are the contact angles $\theta_a(V)$ and $\theta_r(V)$ at the bottom contact lines, which were sliding on the moving bottom plate but stationary with respect to the camera.

Plate fabrication

A simple photolithographic fabrication process was used to prepare EWOD substrates. First, 10/200 nm chromium/gold was evaporated onto silicon wafers. Bottom substrates then received a hydrophobic-coated dielectric (200 nm Teflon AF spin-coated upon 350 nm silicon nitride coated by plasma-enhanced chemical vapor deposition). Top substrates were coated with a thin-film gold but not coated hydrophobic. The exposed gold electrode served two purposes in our experiments. Firstly, it provided electrical ground to the droplet for EWOD. Secondly, the droplet remained stationary (*i.e.* it was not carried away on the moving bottom substrate) by sticking to the gold due to the large measured hysteresis of water on gold ($\theta_r \sim 41°$ and $\theta_a \sim 86°$). Applying a voltage between the stationary top electrode and the moving bottom electrode allowed measurement of dynamic contact angles in the presence of an electrostatic field. This configuration is similar to a demonstrated method used to study wafer coating for immersion lithography.[41]

Experimental setup and procedure

Figure 2 illustrates the overall experimental setup. The top substrate was attached to a vertical micrometer stage, used to precisely control the gap (1 mm in this report) between

the top and bottom plates. The bottom substrate was actuated on a computer-controlled linear stage (Parker LP28 with a PC running Easi-V software), and images of the droplet were captured at 4000 frames per second using a high-speed camera (Phantom v7.2, 800 × 600 pixels) with an optical resolution of 8.1 μm/pixel (note: pixel aspect ratio 1:1). Sufficient lighting was important for achieving high-contrast images of the droplet (see Figure 3a). The amount of light reaching the camera sensor was dependent on the output of light source and the gap between the two plates. We found that it worked well to backlight the droplet using an LED flashlight (Princeton Tec, Impact II) mounted several inches from the plates, which were separated by a gap of 1 mm.

The experimental procedure was as follows: (i) deposit a water droplet (volume ~ 3.14 μL) onto the lower substrate using a pipette, (ii) lower the upper substrate using the vertical micrometer to achieve a 1 mm gap, squeezing the droplet into a disk-like shape having a ~ 2 mm diameter, (iii) Apply DC voltage across the upper (grounded) and lower substrates (positive), and (iv) simultaneously trigger the linear actuator and the high-speed camera. A new droplet of deionized water and fresh surface of the substrate was used for each test. Each speed and voltage pair was tested once, resulting in a total of 92 experiments. No repetitions were performed. Volume loss by evaporation was assumed to have a negligible effect on measurements because the measurement duration was 125 ms. We did not observe volume loss by any other modes, e.g., rivulet formation.

Image analysis

In-house software analyzed the individual frames to obtain a time series of the contact angles. Figure 3a has a cropped raw frame taken from a video of a droplet sliding under 40 V_{DC} at 10 mm/s. The dark region between the green dashed lines is the droplet. Bright regions in the droplet resulted from light passing through the droplet, and dark and light regions outside the green dashed lines are reflections on the top and bottom substrates. In some cases, momentary reflections caused bright spots that obscured the contact line(s); the frames (up to 100 frames in the worst case) affected by such optical errors were manually omitted from analysis. Figure 3b shows a screenshot of the contact angle measurement program, in which advancing and receding angles are simultaneously measured. Upon uploading an image, the software first uses a Canny edge detection technique with a sub-pixel modification[42] to find the droplet menisci. Then, the user inputs the baseline connecting the receding and advancing contact points. Then, the program fits a 2rd order polynomial to 60 points (representing ~50 μm) along the menisci, originating at the contact points. In this way contact angles were measured with ± 0.8° accuracy. This error is equivalent to the variation of measured contact angles when the above processing technique was applied to a video of a static droplet (no sliding plate).

Results and Discussion

Measured (apparent) contact angles

The contact angles measured in our experiments are apparent contact angles, as opposed to the microscopic true contact angles. As the underlying mechanisms leading to measured dynamic angles are not fully understood, macroscopic (apparent) angles cannot be extrapolated to the solid surface in order to infer the corresponding true contact angle.[34] For example, the difference between the apparent and true contact angles on microstructured surfaces has been visualized by sliding a two-dimensionalized droplet on a two-dimensional superhydrophobic surface.[43] Also, the Maxwell stresses at the solid-liquid interface due to EWOD are localized[44] to a distance (~ 1 μm) well below our measurement resolution (~ 100 μm). As result, apparent contact angles not only reflect the influence of contact line

resistance, but also reflect the EWOD force per unit length $f_{drive} = \gamma Ew$ on the x-y plane (the substrate surface), outward normal to the contact line.

Dynamic contact angles

Dynamic contact angle data are presented and discussed using Figures 4 and 5. Before looking at the measured contact angle values, let us examine Figure 4 to gain a qualitative understanding of the observed behaviors, discussed in terms of low and high Ca regimes. We recognize that there is an intermediate regime (roughly $5 \times 10^{-4} < Ca < 10^{-3}$), during which we observe a transition from low to high Ca behaviors. Figure 4 shows meniscus profiles for the lowest and highest sliding speeds (i.e., 1 and 500 mm/s, or $Ca = 1.4 \times 10^{-5}$ and 6.9×10^{-3}, respectively) at 0, 20, and 40 V_{DC}, corresponding to $Ew = 0$, 0.1, and 0.4, respectively. To calculate Ew, we first measured static contact angles at various voltages, then used the data to construct an electrowetting curve ($\cos\theta(V) - \cos\theta$) versus V^2, and finally fit a line to the appropriate range of data (i.e., excluding low voltage data affected by hysteresis and high voltage data affected by saturation). Meniscus profiles were extracted from video frames using ImageJ® edge detection. Figure 4 illustrates an important distinction between low- and high-Ca sliding based on our data: hysteresis is apparently insensitive to EWOD voltage at $Ca < 5 \times 10^{-4}$ when $Ew \leq 0.4$, and hysteresis is voltage-dependent at $Ca > 10^{-3}$ when $Ew \leq 0.4$. Comparing left and right columns, we can clearly see that in the right column increasing voltage causes increased stretching of the droplet in the direction of plate motion, indicating increased resistance to sliding. In contrast, there is no apparent difference in droplet stretching indicated by meniscus profiles in the left column. In this low Ca regime, apparent contact angles may decrease with voltage, but hysteresis does not. Keep in mind that for the initial static situation before sliding commences, the meniscus profiles are symmetrical about the center of the droplet. We can also interpret the data by thinking of dynamic contact angle hysteresis as a result of a kinetic friction force. First imagine there is no friction: the contact angles would be symmetrical at every cross section of the droplet at any sliding speed, so we would observe no hysteresis. In this case we cannot impart a force to the moving substrate by sliding the droplet. Next imagine there is infinite friction: the droplet would not slide, but rather it would stretch until rupture at any sliding speed, so the hysteresis would be immeasurable. Finally, imagine there is finite friction: the droplet is stretched to an extent that indicates the amount of sliding friction. In this case, the force we can impart to the moving substrate by sliding the droplet is related to the surface tension and how much the droplet has been stretched in the sliding direction, which we quantify by dynamic contact angle hysteresis force $\gamma(\cos\theta_r(V) - \cos\theta_a(V))$.

Figure 5(a) summarizes dynamic contact angle data at sliding speeds ranging from 1 to 500 mm/s, corresponding to Ca between 1.4×10^{-5} and 6.9×10^{-3}. Each data point represents the average of contact angles extracted from ~ 500 video frames (representing a duration of 125 ms), and the standard deviations of each average are shown in Figure 5c. In Figure 5a, advancing (right-of-center) and receding (left-of-center) data are plotted versus Ca in logarithmic scale. Note that Ca is a function of contact line velocity (i.e., it is negative for the receding contact line) and its magnitude is assumed equal to the stage speed. As expected, all angles decreased with applied EWOD voltage, and advancing angles increased with speed while receding angles decreased with speed. A higher advancing angle and a lower receding angle, i.e., increased contact angle hysteresis, means a droplet encounters more resistance as it slides faster. Data at the highest voltage (60 V_{DC} or $Ew = 0.9$) are not discussed here because contact line motions were oscillatory and therefore contact line speeds varied significantly from stage speeds. These data are discussed later in a dedicated subsection.

We see a transition at $Ca \approx 10^{-3}$, above which there are clear voltage and speed dependences. For a water droplet, $Ca = 10^{-3}$ corresponds to $v \sim 70$ mm/s, which is commonly achieved by droplets in EWOD devices reported in the literature. For $Ca < 10^{-3}$, the observed dependence of contact angle on sliding speed is weak. In this range, dynamic contact angles change much more by EWOD than by sliding. In the high sliding speed range of $Ca > 10^{-3}$, however, the electrowetting voltage strengthens the dependence on speed. As the sliding speed approaches $Ca = 10^{-2}$, the advancing dynamic contact angle at $Ew = 0.4$ catches up with those at $Ew = 0$ and $Ew = 0.1$, while the receding dynamic contact angle at $Ew = 0.4$ distances itself lower from those at $Ew = 0$ and $Ew = 0.1$. It has not yet been demonstrated that pure water droplets can reach $Ca = 10^{-2}$ under EWOD actuation alone, but we expect that this regime is relevant to a wide range of aqueous surfactant and biochemical solutions, which can have about same hysteresis as water but lower surface tension and higher viscosity (recall $Ca = \eta v/\gamma$).

Figure 5(b) plots the above data to express the difference between the advancing and receding as a dimensionless resistance force per unit length ($\cos\theta_r(V) - \cos\theta_a(V)$) versus Ca. The effect of high sliding speed is most clearly seen: the resistance increases with EWOD voltage if the sliding speed is high. In the low speed range, the resistance to sliding appears to be independent of voltage – this finding supports the previously reported notion that dynamic contact line resistance may be characterized by a voltage-independent coefficient of friction.[10]

Inertial effects

We have stated that the dynamic contact angles reported in Figures 5a were averaged over 500 video frames, spanning 125 ms of droplet sliding, and therefore there is a built-in approximation that the meniscus for this period is quasi-static. For a given experiment, the validity of this approximation is related to the variation in measured contact angles prior to averaging. Figure 5c is plot of standard deviations (SD) of measured dynamic contact angles for $Ew = 0$, 0.1, and 0.4 at all speeds. At $Ew = 0.9$, the quasi-static approximation is inappropriate for all speeds due to the large oscillations of the contact lines. The dimensionless Weber number ($We = v^2 \rho l/\gamma$, where v is the stage speed, $\rho = 1000$ kg/m^3 is the liquid density, and $l = 1$ mm is the plate gap) expresses the relative importance of inertial and surface tension forces; for our experiments We ranges from 1.4×10^{-5} at 1 mm/s to 3.5 at 500 mm/s. In Figure 5c, the SD values at $Ca < 10^{-3}$ ($We \sim 0.07$) are approximately 1° for all voltages, suggesting that inertial effects are minimal. At $Ca > 10^{-3}$, however, the SD values increase with increasing Ca. This clear increase of contact angle variation with stage speed indicates the strengthening influence of inertia, especially under strong electrowetting ($Ew = 0.4$ in Figure 5c). This can be explained as follows. The sudden initial acceleration (fixed at 2 m/s^2) of the stage imposed a force causing sudden deformation of the droplet accompanied by oscillations that remained during steady sliding of the plate, and the amplitudes of said oscillations were larger at higher speeds. A simple scaling analysis based on surface tension and inertial energies, provided in Supporting Information, shows that a characteristic timescale for inertial droplet oscillations in this experimental configuration is about 10 ms. This agrees with our observations of the slight contact angle oscillations (characterized by 1° < SD < 10°) observed at $Ew = 0.4$ and $Ca > 10^{-3}$ as well as bulk droplet oscillations at $Ew = 0.9$, which are discussed in the Supporting Information. Because the inertial timescale is about 10 times less than our experimental timescale (125 ms), we were able to observe several cycles. For this system, the estimated visco-capillary timescale ($\tau_\eta \sim l\eta/\gamma \sim 10$ μs, with viscosity $\eta = 0.001$ Pa·s) is well below the temporal measurement resolution (250 μs), meaning that viscous effects were not significant with respect to the observed oscillations.

Dynamic wetting models

We have compared the usefulness of simplified dynamic contact angle models based on hydrodynamics (Cox-Voinov) and molecular-kinetic theory (MKT) with respect to our data. The details of our fitting procedures, plots, and fitting parameters are included as Supplementary Information. In short, the Cox-Voinov model most faithfully captures the trend of the data at $Ew = 0.4$, which makes qualitative sense given that the contact angles are lowest for these case (data for $Ew = 0.9$ were excluded from this analysis). This result, however, is contradicted by physically unreasonable fitting parameters. Alternatively, the MKT yielded physically reasonable fitting parameters at the advancing contact line, but not at the receding. This lack of symmetry for wetting and de-wetting indicates the failure of the model to capture both processes and suggests perhaps that there is a different balance of dissipation mechanisms at the front and rear of the droplet. As explained recently by Fetzer and Ralston,[45] it may be appropriate to attribute the observed asymmetry of advancing and receding contact angles to microscopic pinning energies. The main conclusion from the analyses based on these simplified theoretical models (i.e., the CV and MKT) is that a more intricate model will be required in order to capture the full range of dynamics associated with droplet sliding under EWOD, especially for cases with high contact angles and low viscosities.

Contact lines de-wetting above a critical velocity become serrated, developing trailing vertices, or corners. At even higher velocities, rivulets or droplets are deposited onto the surface.[46, 47] We did not observe these types of liquid deposition in our experiments, but, with our current experimental setup, we cannot say for sure whether or not a corner was formed at the rear of the droplet. Bertrand et al. provided an estimate for the critical receding dynamic contact angle (θ_c) below which such corners should be expected. Their relationship, $\theta_c = 3\ln(L/a)/(\zeta/\eta)$, Equation 17 in,[46] is a function of a dimensionless ratio, ζ/η, where ζ is a contact-line friction coefficient based on MKT parameters:[46] $\zeta \sim k_B T/\kappa\lambda^3$. Using fitting parameters of the $Ew = 0.4$ advancing contact line (details in Supplementary Information), we have $\zeta \sim 0.08$ Pa·s, and $\zeta/\eta \sim 80$. With $\ln(L/a) = 10$, we may expect trailing corners to form when the receding contact angle is observed to be $\sim 20°$; the fact that we did not measure contact angles below about $45°$ for $Ew \le 0.4$ might suggest that there were no corners, but this is highly speculative considering the uncertainty of the MKT fitting parameters.

Stick-slip motion

The contact lines were not stable for experiments at 60 V_{DC} ($Ew = 0.9$). While the periodic motions described in this subsection are interesting, the associated contact angle data, being oscillatory, are not included with our main results (Figure 5). We observed periodic pinning (stick) and rapid forward recovery (slip) of the wetting line. For slow sliding speeds, i.e. $Ca < 5\times10^{-4}$, advancing angles oscillated between $\sim 60°$ and $\sim 90°$, and the wetting line travelled about 0.3 mm. Within a few milliseconds after the recovery slip of the advancing line, the receding line slipped forward as well. Figure 6 provides the meniscus profiles during a representative experiment, in which the stage moved left at 3 mm/s. The lines are numbered to indicate moments in time, where '1' is the moment prior to slip, '2' is the moment after the advancing line has slipped, and '3' is the moment after the receding contact line has slipped, occurring a few milliseconds after '2'. A transition from state '3' to '1' completes the cycle. During this later stage, i.e., '3' to '1', advancing and receding contact lines are pinned, i.e., they have zero velocity relative to the bottom plate. With a contact line acceleration measured to be $a \approx 1000$ m/s^2 on average during slip ('1' to '2'), the associated capillary length is $\lambda_c \sim (\gamma/\rho a)^{1/2} \sim 0.3$ mm, which agrees with the observed slip displacement.

Figure 7 summarizes periodic motions observed at $Ew = 0.9$ for low- and high-Ca sliding in terms of contact angles, contact line locations (B_1, B_2, T_1, and, T_2), and droplet shear δ (defined in Figures 1b and 1c). Time histories of contact angles for six intermediate sliding speeds ($1.4\times10^{-4} \leq Ca \leq 8.2\times10^{-4}$) are provided in the Supporting Information to show the transition from large- to small-amplitude stick-slips. By examining the contact angles in the top row, we observe a momentary negative hysteresis at 3 mm/s. Time histories of the contact line points, T_1, T_2, B_1, and B_2 are plotted on the second row, and those of the droplet shear δ are on the third rows. The droplet shear δ represents the position of the bottom wetted area relative to the top along the x-axis (see Figures 1b and 1c) and is defined to be positive when the bottom wetting area is trailing the top wetted area. While the slow-speed case (left column) is characterized by large-amplitude stick-slips, the high-speed case (right column) is characterized by inertial bulk droplet oscillations. A simple spring-mass scaling analysis of this motion is provided in the Supporting Information.

Summary

We have designed and implemented an experiment to measure both advancing and receding dynamic contact angles under EWOD as function of droplet sliding speed. Covering ranges of Ew and Ca relevant to EWOD droplet microfluidic systems, the obtained data led us to the relationships between the dynamic contact angle hysteresis and sliding speed or EWOD voltage. Our results show that for $Ca < 5\times10^{-4}$, contact angle hysteresis has no apparent voltage dependence and a weak variation with sliding speed. When $Ca > 10^{-3}$, however, contact angle hysteresis is strongly voltage- and speed-dependent. At $Ew = 0.9$, we observed large-amplitude stick-slip motions when $Ca < 5\times10^{-4}$.

Supplementary Material

Refer to Web version on PubMed Central for supplementary material.

Acknowledgments

References

1. de Gennes PG. Rev Mod Phys. 1985; 57:827–863.

2. de Gennes, PG.; Brochard-Wyart, F.; Quéré, D. Capillarity and Wetting Phenomena: Drops, Bubbles, Pearls, Waves. Springer; New York: 2004.

3. Robbins MO, Joanny JF. Europhys Lett. 1987; 3:729–735.

4. Gao L, McCarthy TJ. Langmuir. 2006; 22:6234–6237. [PubMed: 16800680]

5. Li F, Mugele F. Appl Phys Lett. 2008; 92:244108–244111.

6. Lee J, Moon H, Fowler J, Schoellhammer T, Kim CJ. Sensors and Actuators A. 2002; 95:259–268.

7. Cho SK, Moon H, Kim CJ. Journal of Microelectromechanical Systems. 2003; 12:70–80.

8. Pollack MG, Fair RB, Shenderov AD. Appl Phys Lett. 2000; 77:1725–1726.

9. Mannetje, DJCMt; Murade, CU.; van den Ende, D.; Mugele, F. Appl Phys Lett. 2011; 98:014102.

10. Beni G, Tenan MA. J Appl Phys. 1981; 52:6011–6015.

11. Suzuki S, Nakajima A, Kameshima Y, Okada K. Surf Sci Lett. 2004; 557:L163–L169.

12. Petrov PG, Petrov JG. Colloids Surf. 1991; 61:227–240.

13. Petrov JG, Petrov PG. Colloids Surf. 1992; 64:143–149.

14. Schertzer MJ, Gubarenko SI, Ben-Mrad R, Sullivan PE. Langmuir. 2010; 26:19230–19238. [PubMed: 21080633]

15. Blake TD, Clarke A, Stattersfield EH. Langmuir. 2000; 16:2928–2935.

16. Moon H, Cho SK, Garrell RL, Kim CJ. J Appl Phys. 2002; 92:4080–4087.

17. Lin YY, Evans RD, Welch E, Hsu BN, Madison AC, Fair RB. Sensors Actuators B. 2010; 150:465–470.

18. Chang JH, Choi DY, Han S, Pak JJ. Microfluid Nanofluid. 2010; 8:269–273.

19. Li Y, Parkes W, Haworth LI, Ross AWS, Stevenson JTM, Walton AJ. J Microelectromech Syst. 2008; 17:1481–1488.

20. Berthier, J. Microdrops and Digital Microfluidics. William Andrew Inc.; Norwich, NY: 2008.

21. Baviere R, Boutet J, Fouillet Y. Microfluid Nanofluid. 2008; 4:287–294.

22. Beni G, Hackwood S, Jackel JL. Applied Physics Letters. 1982; 40:912–914.

23. Hayes RA, Feenstra BJ. Nature. 2003; 425:383–385. [PubMed: 14508484]

24. Lee J, Kim CJ. Journal of Microelectromechanical Systems. 2000; 9:171–180.

25. Brzoska JB, Brochard-Wyart F, Rondelez F. Langmuir. 1993; 9:2220–2224.

26. Darhuber AA, Valentino JP, Troian SM, Wagner SJ. Microelectromechanical Systems. 2003; 12:873–879.

27. Jun TK, Kim CJ. J Applied Physics. 1998; 83:5658–5664.

28. Sammarco TS, Burns MA. AIChE Journal. 1999; 45:350–366.

29. Brochard F. Langmuir. 1989; 5:432–438.

30. Ren H, Fair RB, Pollack MG, Shaughnessy EJ. Sensors and Actuators B. 2002; 87:201–206.

31. Blake, TD. Wettability. Berg, JC., editor. Marcel Dekker, Inc.; New York: 1993. p. 251-309.

32. Blake TD, Haynes JM. Journal of Colloid and Interface Science. 1969; 30:421–423.

33. Brochard-Wyart F, deGennes PG. Advances in Colloid and Interface Science. 1992; 39:1–11.

34. Blake TD. J Colloid Interface Sci. 2006; 299:1–13. [PubMed: 16631781]

35. Kim HY, Lee JH, Kang BH. J Colloid Interface Sci. 2002; 247:372–380. [PubMed: 16290477]

36. Extrand CW, Kumagai Y. J Colloid Interface Sci. 1997; 191:378–383. [PubMed: 9268520]

37. Sakai M, Song JH, Yoshida N, Suzuki S, Kameshima Y, Nakajima A. Surf Sci Lett. 2006; 600:L204–L208.

38. Nelson, W.; Sen, P.; Kim, CJ. Proc Solid-State Sensors, Actuators and Microsystems Conference; Denver, CO. 21-25 June 2009; 2009. p. 2014-2017.Denver, CO, 2009

39. Walker SW, Shapiro B. J Microelectromech Syst. 2006; 15:986–1000.

40. Walker SW, Shapiro B, Nochetto RH. Phys Fluids. 2009; 21:102103–102129.

41. Schuetter S, Shedd T, Doxtator K, Nellis r. J Microlith, Microfab, Microsyst. 2006:5.

42. Sen, P. Ph D Dissertation. University of California; Los Angeles: 2007.

43. Chen, Z.; Kim, CJ. Proc Int Conf Miniaturized Systems of Chemistry and Life Sciences. Jeju, Korea: Nov. 2009 p. 1362-1364.Jeju, Korea, Nov. 2009

44. Mugele F, Buehrle J. J Phys: Condens Matter. 2007; 19:375112–375132.

45. Fetzer R, Ralston J. J Phys Chem C. 2009; 113:8888–8894.

46. Bertrand E, Blake TD, DeConinck J. Coll Surf A. 2010; 369:141–147.

47. Bonn D, Eggers J, Indekeu J, Meunier J, Rolley E. Rev Mod Phys. 2009; 81:739–805.

(a)

(b)

(c)
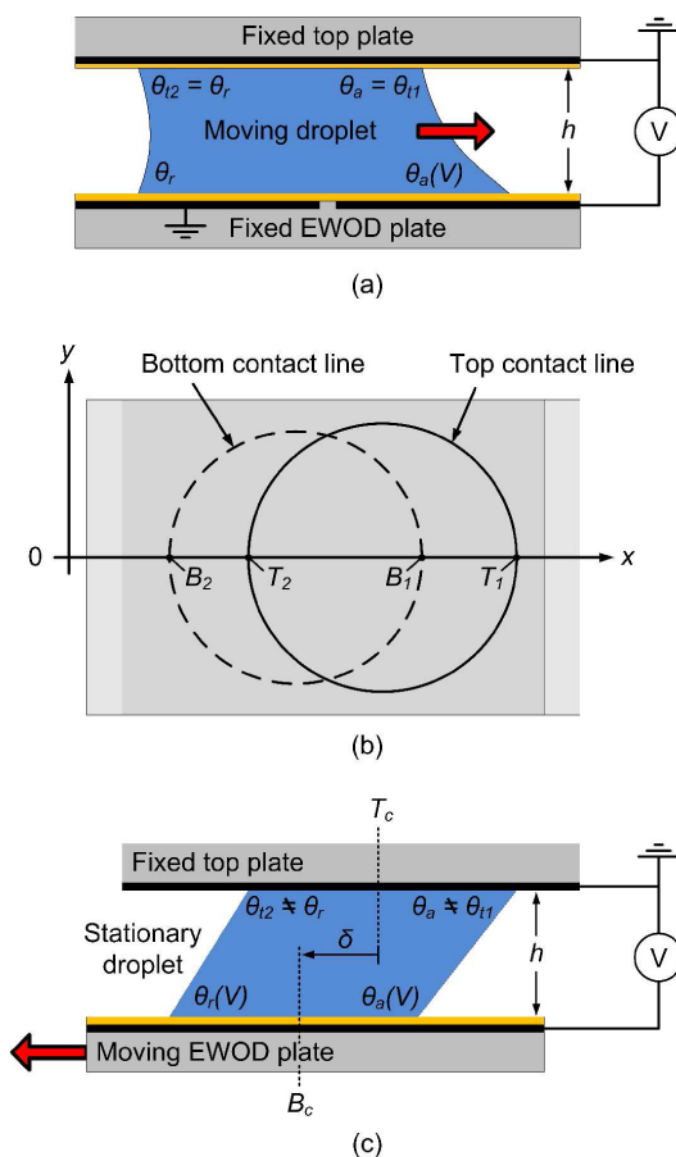
Figure 1.
(a) Schematic cross section of typical parallel-plate EWOD droplet actuation. (b) Top view and (c) cross section A-A′ of the concept of our experiment: A stationary droplet sits on a hydrophobic-coated dielectric, which moves left. The droplet sticks to a top hydrophilic electrode. Upper and lower contact angles, θ, at the center cross-section of each droplet are shown. Subscripts 'a' and 'r' denote advancing and receding, and superscripts '$t1$' and '$t2$' indicate right and left top plate angles. T_1, T_2, B_1, and B_2 are contact points at $y = 0$, as shown in the top view. T_c and B_c are located at the midpoints of segments T_1T_2 and B_1B_2 and used to define parameter δ in the cross section view.
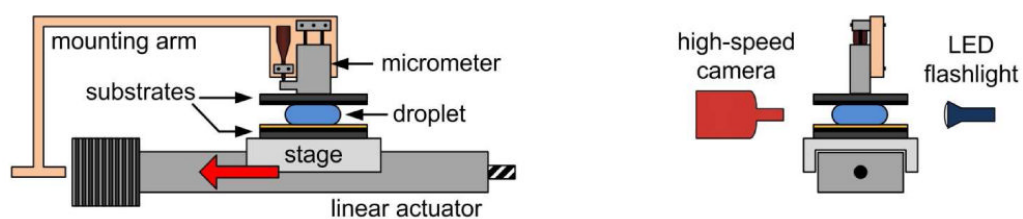
Figure 2.
Schematic views of the experimental setup. The linear actuator is controlled using a computer. The high-speed camera captures images at 4000 frames per second (fps).
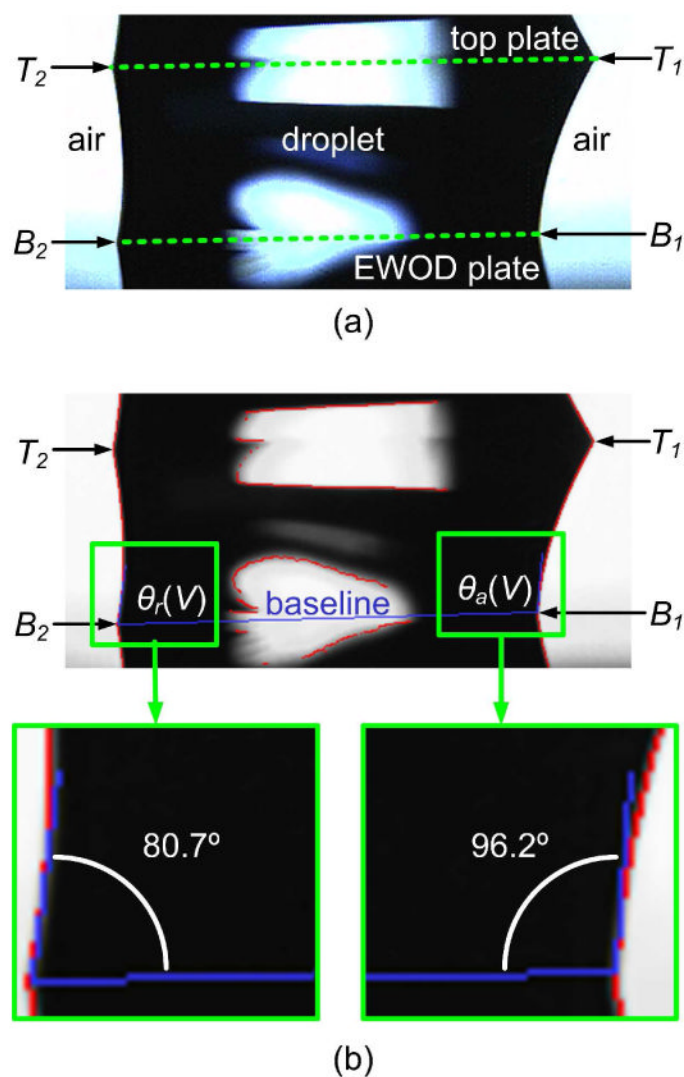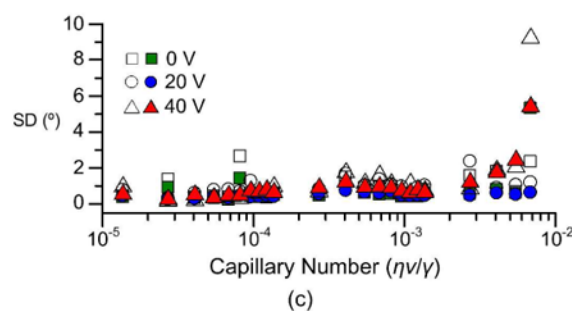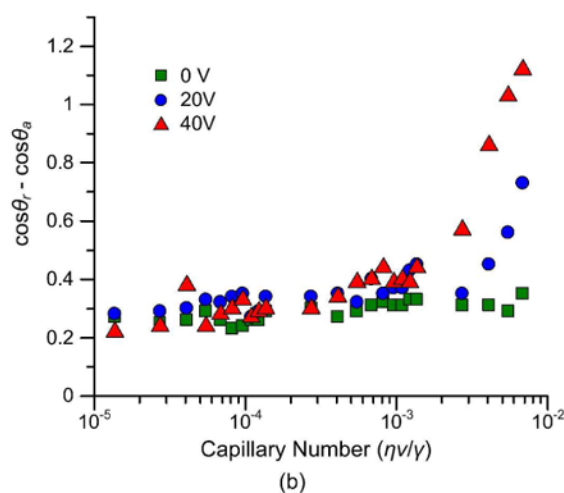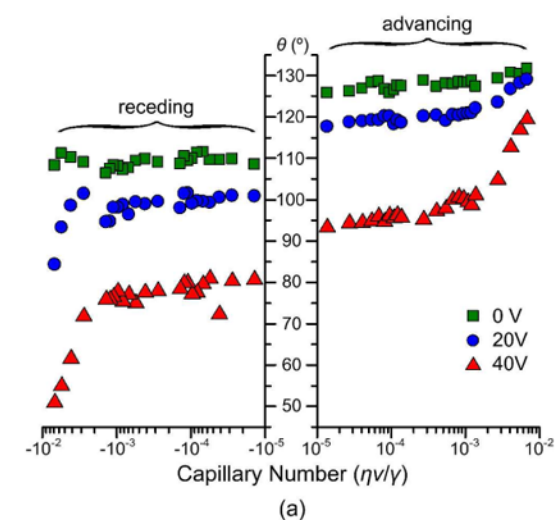
Figure 3.
(a) Cropped raw image of a droplet sliding on the EWOD plate moving at 10 mm/s. (b) Screen shot of the image processing software and close-ups of contact point regions. Red lines indicate the software edge detection, and blue lines indicate the baseline and contact angles.
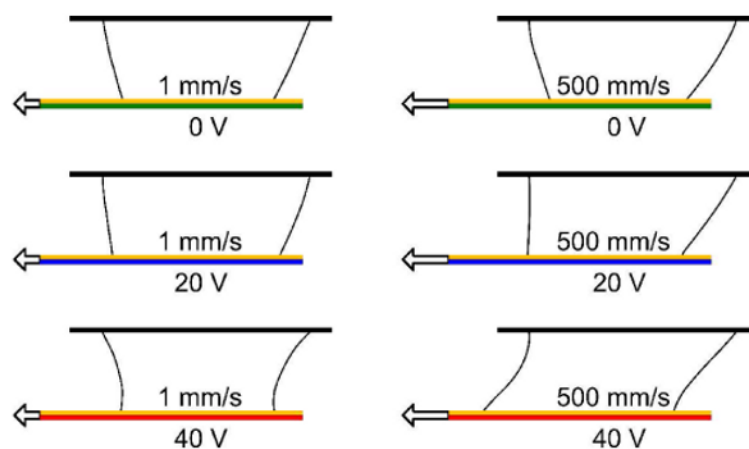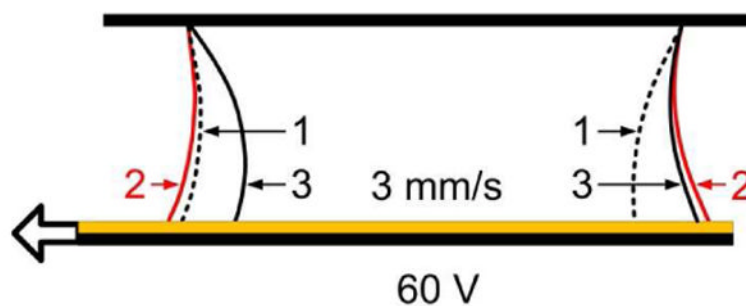
Figure 4.
Side view meniscus profiles of droplets moving at 1 and 500 mm/s. Profiles were obtained using edge detection in ImageJ.
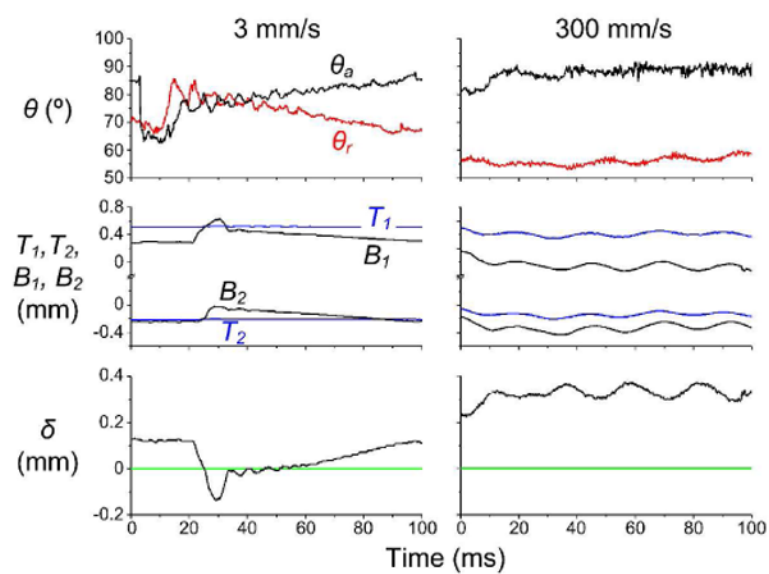
Figure 5.
(a) Measured dynamic contact angles at various EWOD voltages versus capillary number $Ca = \eta v/\gamma$. Every data point is an average of ~500 images. (b) Dimensionless force per unit length $f_{hyst}/\gamma = \cos\theta_r - \cos\theta_a$. (c) Standard deviations (SD) of contact angle measurements.

Figure 6.
Side view meniscus profiles showing stick-slip motion occurring on the EWOD plate of 60 V_{DC} ($Ew = 0.9$) moving at 3 mm/s ($Ca = 4.1 \times 10^{-5}$) to the left. The lines are numbered to indicate moments in time, where '1' is the moment prior to slip, '2' is the moment after the advancing line has slipped, and '3' is the moment after the receding contact line has slipped, occurring a few milliseconds after '2'. A transition from state '3' to '1' completes the cycle. Profiles were obtained using edge detection in ImageJ.

Figure 7.
Plots of dynamic contact angles, contact points T_1, T_2, B_1, and B_2, and displacement parameter δ for 3 mm/s and 300 mm/s sliding speeds. Time scales are the same for all plots, and vertical axis scales are the same for each row.